

Efficient Navigation of Active Particles in an Unseen Environment via Deep Reinforcement Learning

Yuguang Yang,^{a,b} Michael A. Bevan,^b Bo Li^{a*}

^a *Institute of Biomechanics and Medical Engineering, Applied Mechanics Laboratory,
Department of Engineering Mechanics, Tsinghua University, Beijing 100084, China*

^b *Chemical & Biomolecular Engineering, Johns Hopkins University, Baltimore, MD
21218*

Abstract

Equipping active particles with intelligence such that they can efficiently navigate in an unknown complex environment is essential for emerging applications like precision surgery and targeted drug delivery. Here we develop a deep reinforcement learning algorithm that can train active particles to navigate in environments with random obstacles. Through numerical experiments, we show that the trained particle agent learns to make navigation decision regarding both obstacle avoidance and travel time minimization, relying only on local pixel-level sensory inputs but not on pre-knowledge of the entire environment. For arbitrarily long distance in unseen complex obstacle environments, the trained particle agent can nearly optimally navigate at a fixed computational cost. This study illustrates the potentials of employing artificial intelligence to bridge the gap between active particle engineering and emerging real-world applications.

Keyword: active particle | artificial intelligence | navigation | deep reinforcement learning

* Corresponding author.

E-mail address: libome@tsinghua.edu.cn (B. Li).

Self-propelled active particles have recently demonstrated great promise as the next generation of micro-robots to work in complex environment for tasks like drug delivery, precision surgery, search, and environmental remediation.¹⁻⁵ Efficient navigation in complex environments with real-world complexities, for example, unseen obstacles and dead-ends, large-scale navigation distance, plus additional time and fuel constraints, is crucial for practical applications. Towards this end, besides the progress in developing faster active micro-robots^{2,6}, various efforts have been made to develop better navigation strategies.⁷⁻¹¹ For example, Markov decision process framework⁸ and variational Fermat's principle¹¹ are used to compute the optimal navigation path in mazes and flow fields.

However, the above-mentioned methods generally require pre-knowledge of the entire environment and the computational cost often increases dramatically for large length-scale navigational tasks. In the real-world applications where micro-robots need to travel long distances (e.g., tissue, soil, and vessels) in an unacquainted or spatiotemporally changing environment, either the pre-planned paths/strategies will break down or high computational cost is prohibitive. Therefore, one pressing challenge to steer micro-robots for real-world applications is the efficient navigation within an unknown, complex, and large length-scale environment.

Recently, deep reinforcement learning (DRL), inspired by the animal learning process, has achieved remarkable performance in various domains that require sequential decisions, ranging from games^{12,13} and robotics^{14,15} in traditional computer science to novel applications like drug design¹⁶, chemical reaction optimization¹⁷, medical treatment¹⁸, and collective swimming strategy¹⁹. The usage of deep neural networks, particularly the convolutional neural network²⁰, has significantly expanded the success of traditional reinforcement learning to challenging domains suffering from dimensionality curse because it enables the learning of efficient representation from high-dimensional observations and facilitates the generalization of experiences to new situations.

In this Letter, we present a DRL algorithm that can train an active particle agent to learn the navigation strategies in complex environments. We consider a Brownian-type active particle that can self-propel via either internal or external energy injection yet without control on its orientation. Our goal is to train an active particle agent that can make optimal sequential self-propulsion decision to navigate through environments with random obstacles and traps, using the image of its local observation and target position as sensory inputs [Fig. 1(a)]. The usage of pixel-level raw sensory inputs can train the active agent to accommodate visually rich environments and work naturally with real-world sensors such as microscopes. Further, the trained agent can navigate in arbitrary large environments at a fixed computational cost, since only local information is used. Training an intelligent particle to master the rule of efficient navigation based on local visual information, in contrast to developing algorithms to compute navigation strategy on a case by case basis, naturally resembles how a human being makes navigation decisions. Considering an adult first time arrives in a city that he has never been there before, he will have no trouble in traversing the building blocks and taking short-cut whenever possible.

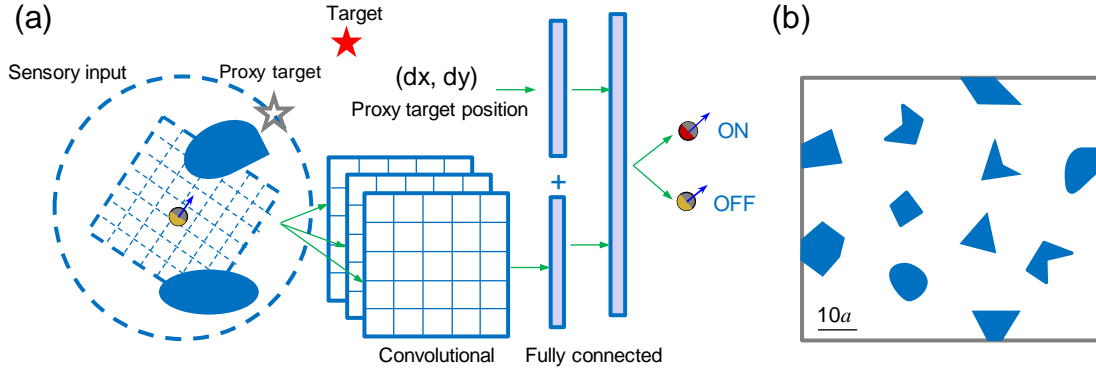


Figure 1 (a) The neural network architecture used to approximate the optimal Q function in our DRL algorithm. The details of the architecture are in the *supporting information*. Two streams of sensory inputs are fed to the neural network. One input consisting of a 30×30 binary image sensing from the square-shaped neighborhood of the particle is fed into convolutional layers. Another input consisting of the target's position is fed into a fully connected layer. A distant target will be transformed into a local proxy target. Two sources of inputs then merge and enter a fully connected layer. The final layer will output two values corresponding to the Q values of the ON and OFF actions. (b) The obstacle environment used to train the particle agent.

By training the agent to navigate in a small-sized example environment [Fig. 1(b)], we show that the trained agent can later navigate efficiently in large-sized complex environments with obstacles of unseen shapes and arrangement. We illustrate that the neural network can learn effective representations of observations and thus shed light on the underpinnings of the successful navigation performance. Our results show the great potential of employing cutting-edge deep learning methods to aid real-world applications of active particles.

We model the motion of a self-propelled particle confined on a plane by

$$\begin{aligned}\partial_t x &= \xi_x(t) + v \cos \theta, \\ \partial_t y &= \xi_y(t) + v \sin \theta, \\ \partial_t \theta &= \xi_\theta(t),\end{aligned}\tag{1}$$

where x , y , and θ denote the position and orientation, t is time, and v is propulsion speed taking binary values of 0 and v_{\max} as the control inputs (denoted by OFF and ON). Brownian translational and rotational displacement processes ξ_x , ξ_y , and ξ_θ are zero-mean Gaussian noise process with variances $\langle \xi_x(t) \xi_x(t') \rangle = 2D_t \delta(t-t')$, $\langle \xi_y(t) \xi_y(t') \rangle = 2D_t \delta(t-t')$, and $\langle \xi_\theta(t) \xi_\theta(t') \rangle = 2D_r \delta(t-t')$, respectively, where D_t is the translational diffusivity and D_r is the rotational diffusivity. Throughout this work, lengths are normalized by particle radius a and time is normalized by $\tau = 1 / D_r$. Control update time is $t_c = 0.1 \tau$, integration time step $\Delta t = 0.001 \tau$, and $v_{\max} = 2a / t_c$. Note that the orientation θ is subject to Brownian rotation and not allowed to be controlled.

We denote the particle state by $s_n = (x_n, y_n, \theta_n)$. The observation $\phi(s_n)$ at s_n consists of the pixel image of the particle's neighborhood and the target position (x^t, y^t) , as shown in Fig. 1(a). We use the reinforcement learning framework to seek an optimal control policy, π^* , which maps an observation $\phi(s_n)$ to a self-propulsion action (i.e. ON or OFF) such that the expected reward accumulated during a navigation process

$\mathbb{E} \sum_{n=0}^{\infty} \gamma^n [R(s_n)]$ is maximized, where R is the one-step reward function and γ is the

discount factor setting to be 0.99. To seek an optimal policy minimizing arrival time^{8,21}, R is set equal to 1 for all states that are within a threshold distance 2 to the target and 0

otherwise. Our DRL algorithm uses a deep convolutional neural network [Fig. 1(a)] to approximate the optimal action-value function (known as Q function) given by

$$Q^*(\phi(s), v) = \mathbb{E} \left[R(s_0) + \gamma^1 R(s_1) + \gamma^2 R(s_2) + \dots \mid \phi(s_0) = \phi(s), v_0 = v, \pi^* \right]. \quad (2)$$

The agent is only trained via back-propagation²² to navigate in a free-space environment and an environment with obstacles of different shapes [Fig. 1(b)]. During training, starting points and targets are randomly generated to expose the agent to diverse situations. With the learned optimal Q^* function, optimal propulsion decision at a given observation $\phi(s)$ is given by $v^* = \operatorname{argmax}_v Q^*(\phi(s), v)$. The agent is trained using canonical deep Q learning algorithm²³ with several enhancements^{24,25} to speed up the convergence (see *supporting information* for more details).

Motivated by recent breakthroughs in visual image understanding via deep convolution neural networks^{20,26}, sensory information of the particle neighborhood, represented by a $W \times W$ binary image ($W = 30$), is fed into convolutional layers [Fig. 1(a)]. The target's position in the particle's local coordinate system is fed into a fully connected layer. One critical treatment for distant targets (distance $> W$) is that they are transformed into local proxy targets with distance W (i.e., cutoff threshold W). The complete reliance on local information (i.e., neighborhood and local proxy target) is the foundation that our DRL algorithm can readily apply to navigations of arbitrary length scales at fixed computation cost. Finally, these two sources of sensory inputs merge and enter a fully connected layer. The last layer will output the two Q values associated with the ON and OFF actions.

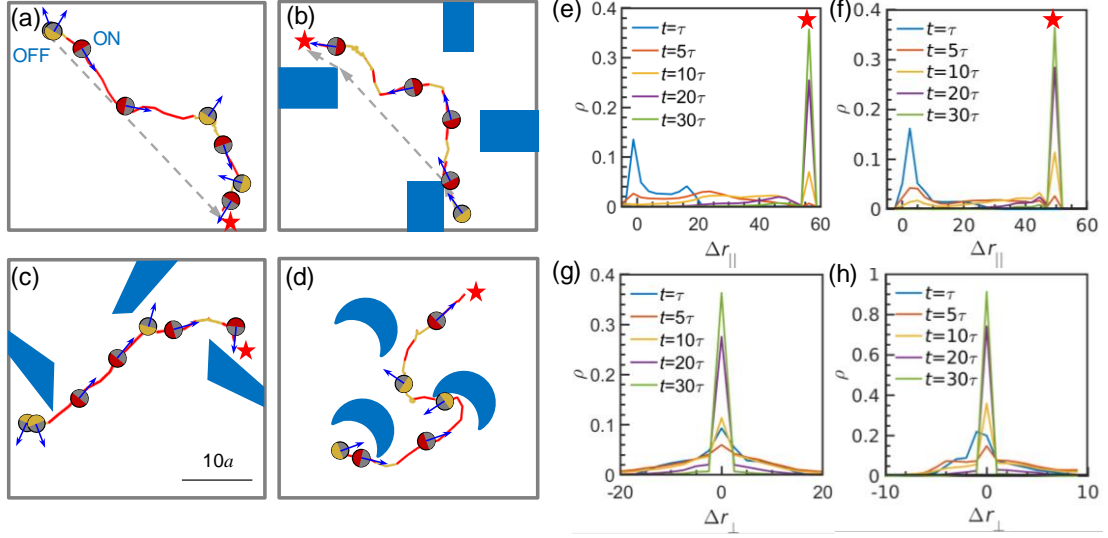


Figure 2 Navigation trajectories of DRL trained active particles in different environments, including (a) free space, (b) rectangle obstacles, (c) reentrant rectangle obstacles, and (d) moon-shape obstacles. Targets are denoted by red pentagrams. Trajectories are colored red when self-propulsion is turned ON and are colored gold when self-propulsion is turned OFF. Grey dash vectors are global shortest path from the starting point to the target. (e–h) The distributions of parallel and perpendicular components of displacements when navigating in free space (e, g) and in rectangle-obstacle environment (f, h).

The trained DRL active particle agent can efficiently navigate in free space and obstacle environments that are unseen during its training process [Fig. 2(a–d)]. In free space navigation [Fig. 2(a)], the trained particle agent has learned an ‘orientation timing’ strategy where it will propel itself when the target locates in front or otherwise wait for the favorable orientation to be sampled by Brownian rotation. The navigation strategy derived from the learned optimal Q^* function can be summarized approximately via

$$\pi^*(s) = \begin{cases} v_{\max}, & d_n \in [d_c, \infty), \\ v_{\max}, & d_n \in [0, d_c), \alpha_n \in [-\alpha_c, \alpha_c], \\ 0, & \text{otherwise.} \end{cases} \quad (3)$$

where d_n is the projection of the target-particle vector onto the orientation vector $\mathbf{n} = (\cos\theta, \sin\theta)$, α_n is the angle between target-particle distance vector and \mathbf{n} , and parameter d_c and α_c are fitted to be $\sim 0.4v_{\max}t_c$ and $\sim 30^\circ$. Successful navigation in unseen environments with obstacles of different shapes and arrangements, including regular

rectangle obstacles [Fig. 2(b)], reentrant rectangle obstacles [Fig. 2(c)], and moon-shaped obstacles [Fig. 2(d)], indicates the trained particle agent has learned generic navigation principles generalizing beyond the training environment [Fig. 1(b)]. Specifically, the agent learns to wait for desired orientations to propel itself around convex blocking obstacles [Figs. 2(b)(c)] or temporally propel itself away from concave traps [Fig. 2(d)]. In general, the agent can smartly avoid the obstacles and approximately follow the shortest geometric path towards the target, even when obstacles are partially observed (i.e., only part of the obstacle is in the sensory window).

We examine the distribution of displacements under DRL control during the navigation processes in [Fig. 2(a) and (b)]. In collecting the statistics, trajectories are starting at the same initial position but with randomly sampled initial orientations. The displacements at different times are projected along and perpendicular to the shortest geometric path (represented by the direction vectors connecting from the initial position to the target), which are used to capture the navigation progress and the deviation from the ideal direct path, respectively. As shown in Fig. 2(e) and (f), for navigation in both free space and rectangle-obstacle environment, the displacement distributions exhibit two modes at $t = \tau$: (i) a near mode located at 0 is because trajectories with unfavorable initial orientations are waiting around the initial position for favorable orientations from stochastic rotation sampling; (ii) a far mode located at $\sim 0.75v_{\max}\tau$ is because trajectories with favorable initial orientation rapidly self-propel. At longer time, the near mode continues to spread out and the far mode propagates towards the target, indicating that the trained agent can readily propel itself to get closer to the target when favorable orientation and position appears via Brownian motion. In addition, the perpendicular displacement (i.e., the vertical deviation to the ideal path) distributions exhibit a narrow peak around 0 but with tails extending to $\sim v_{\max}\tau$ in free space and $\sim 0.5 v_{\max}\tau$ in obstacle environment, indicating the DRL trained agent can usually maintain a close distance to the ideal path but occasional large deviation can also occur [Fig. 2(g) and (h)].

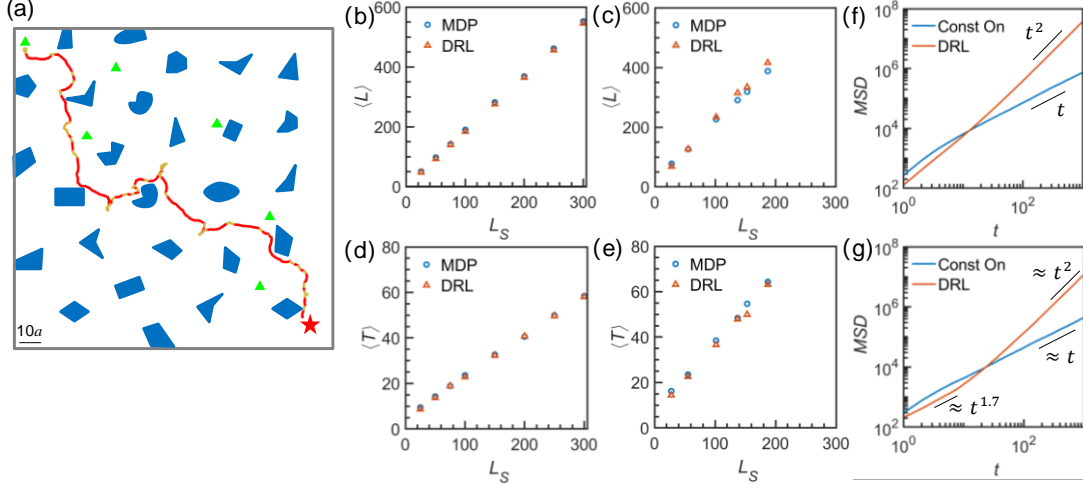


Figure 3 (a) An unseen large-sized test environment used for performance analysis. Solid curve shows an example trajectory of a DRL trained agent navigating from the upper left starting point to the target. (b-e) Mean traveled path length $\langle L \rangle$ and mean first arrival time $\langle T \rangle$ are compared for a DRL and a MDP trained agent navigating in free space (b,c) and in obstacle environment (d,e). Navigations from different starting points (green symbols in (a)) to the prescribed target are analyzed. These different navigation tasks can be parameterized by the shortest geometric path length L_s from starting points to the target. (f, g) The mean squared displacement (MSD) for a DRL trained agent and a constantly self-propelled particle in free space (f) and in periodic obstacle environment (g).

We now systematically quantify navigation performance across different length scales [Fig. 3(a)]. We first benchmark the navigation performance with the model-based Markov decision process (MDP) algorithm (see *supporting information*)^{8,27}, which can compute the optimal navigation strategy using a discretized particle dynamic model. MDP cannot be applied to unseen environment navigation (as it requires pre-knowledge of the environment) nor large-scale navigation tasks (prohibitive computational cost). The performance of DRL and MDP algorithms are compared based on mean traveled path length $\langle L \rangle$ and mean first arrival time $\langle T \rangle$. The traveled path length of a trajectory

is defined by $L = \sum_{i=1}^{N-1} \sqrt{(x_{i+1} - x_i)^2 + (y_{i+1} - y_i)^2}$, where $(x_1, y_1), (x_2, y_2), \dots (x_N, y_N)$ are

particle positions observed at consecutive control update times. For trained agents navigating different distances in both free space and the obstacle environment [Fig. 3(a)], DRL trained agent and MDP trained agent perform similarly in terms of traveled path length [Fig. 3(b)(c)] and arrival time [Fig. 3(e)(f)]. Since the MDP agent is known

to seek global optimal performance by planning global shortest paths, the comparable performance indicating that local path planning in DRL agent leads to approximately global optimal performance even it has no access to global environment information. The average travel speeds $v = \langle L \rangle / \langle T \rangle$ are $\sim 0.36v_{\max}$ for navigation in the obstacle environment, smaller than $\sim 0.5v_{\max}$ in free space, as the existence of obstacle prevent the particle to propel as frequent as in free space.

To ultimately evaluate the performance in infinitely-large environments, we examine the mean squared displacement (MSD) for particle navigating towards remote targets in the periodic environment of Fig. 4(a) (see *supporting information*). At both shorter and longer time scale t compared to τ , the MSD of the trained agent particle navigating in free space follows $MSD(t) \sim t^2$ [Fig. 3(f)], as the navigation strategy causes intermittent directed transport towards the target. As a contrast, a constantly self-propelled particle behaves as $MSD(t) \sim t^2$ at shorter time scale due to propulsion and $MSD(t) \sim t$ at longer time when randomized orientation leads to an effective random walk.²⁸ Surprisingly, for navigations in the obstacle environment [Fig. 3(g)], the DRL trained agent particle still displays approximately $MSD(t) \sim t^2$ at longer time scale, although at smaller time scale it displays $MSD(t) \sim t^{1.7}$ with the smaller exponents arises from detours when circumventing obstacles; whereas a constantly self-propelled particle gives approximately $MSD(t) \sim t$ at longer time scale. The similar scaling in MSD indicates that the trained agent can perform directed transport in obstacle environments as efficiently as in free space, although at a smaller travel speed.

Finally, we examined the representations learned from high dimensional sensory inputs by the neural network to understand the successful performance in the previous navigation tasks. We consider an unseen environment with only one obstacle and apply the nonlinear dimension reduction t-SNE algorithm²⁹ to embed the learned representations in the last hidden layer into a 2D plane [Fig. 4(a)]. Each 2D point is colored by the state value defined by

$$V(s) = \max_v Q^*(\phi(s), v) = \mathbb{E}[R(s_0) + \gamma^1 R(s_1) + \gamma^2 R(s_2) + \dots | \pi^*], \quad (4)$$

where $V(s)$ can be interpreted as the expected reward accumulated following the optimal navigation policy. A particle state with higher V indicates this state can arrive at the target faster than other states with lower V .

As shown in Fig. 4(a), high dimensional sensory observations at different particle states are embedded in the 2D plane apparently based on the shortest path distance to the target location (in the horizontal direction) and the particle's orientation (in the vertical direction). Particle states with the shortest distance and favorable orientations are placed to leftmost end with highest state value [Fig. 4(a₁)], while particle states with larger distance are placed slightly to the right with lower state values [Fig. 4(a₂)]. Particle states with intermediate range to the target are placed in the middle with intermediate state value and located at the upper part if the particle favorably orients to the target [Fig. 4 (a₃)] or lower part if the particle orients opposite to it [Fig. 4(a₄)]. For particles located farthest to the target due to the blockage of the obstacle, their observations are assigned to the lowest state value and placed on the rightmost end at either upper or lower wings [Fig. 4(a₅) and (a₆)]. While Q function assigns a lower value to states with unfavorable orientations for particles within an intermediate range, it assigns similar state values to distant particle states regardless of their orientations; this is because initial orientation does not add appreciable value to long-distance navigation. Therefore, as demonstrated in the toy example [Fig. 4a], the reward signals have shaped the neural network to learn representations from observations that can distinguish whether one particle state is more favorable than the other and assign it with higher state value.

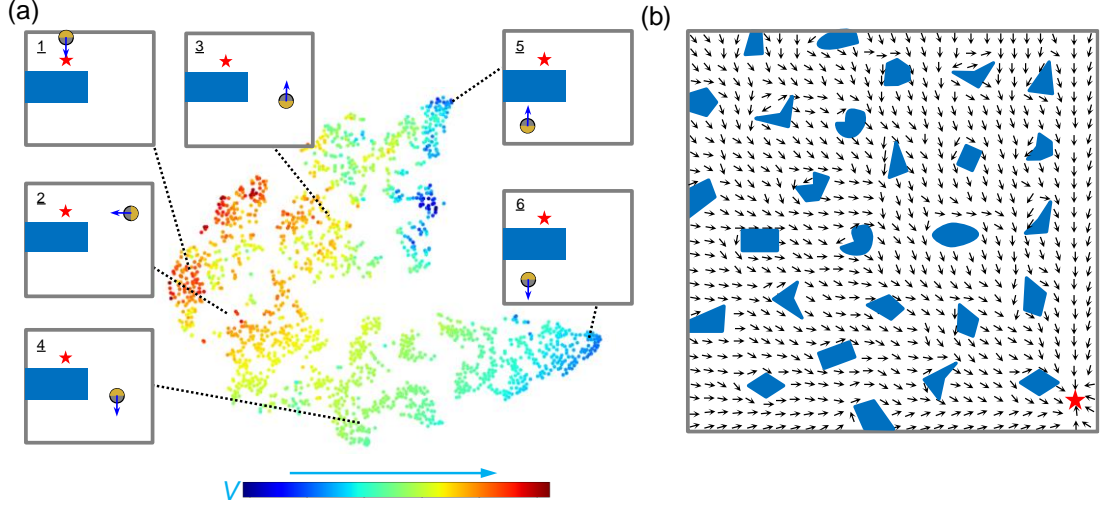


Figure 4 (a) Two-dimensional t-SNE embedding of the representation in the last hidden layer of the neural network in a single obstacle navigation task. Every point corresponds to 2d representation of observations at admissible particle states (x, y, θ) discretized with step size $(1, 1, \pi/8)$. Points are colored by state value (Eq.(4)). (b) Implied navigation direction from the gradient of orientation averaging optimal state value with the target denoted by red pentagram.

Another way to understand the navigation strategy learned by the particle agent is by visualizing the normalized gradient vector (see *supporting information*) of orientation averaging optimal state values $V_{XY}(x, y)$ defined by

$$V_{XY}(x, y) = \frac{1}{8} \sum_{i=1}^8 V(x, y, \frac{i\pi}{4}). \quad (5)$$

As the reinforcement learning algorithm works by specifying the agent to take actions to move a particle from states with low V (e.g., particle states with unfavorable orientation and far away from the target) to states with high V (e.g., particles states with favorable orientation and smaller distance to the target). The gradient of $V_{XY}(x, y)$ represents the effective navigation direction that the trained agent learns to move. In Fig. 4(b), the effective navigation direction in the complex test environment clearly shows the intent to circumvent obstacles and get to the target without any unnecessary detours.

In summary, we have used DRL methodology to tackle the challenge of efficient navigation of active particles in an unseen, partially observable complex environment. The proposed deep convolution neural network allows an active particle agent to learn useful representation from visually rich high-dimensional sensory input and exhibits excellent generalization performance. Although this algorithm is applied in a simplified self-propelled particle model, it can be adapted to active particles with different forms of dynamics^{30,31} or more realistic physics (e.g., hydrodynamics³²). DRL can also be extended to multi-agent system³³ to control multiple active particles to cooperate on tasks and assemble to non-equilibrium machines and devices³⁴.

Acknowledgements

Support from National Natural Science Foundation of China (Grant No. 11672161) is acknowledged.

References

- 1 Li, J., de Ávila, B. E.-F., Gao, W., Zhang, L. & Wang, J. Micro/nanorobots for biomedicine: Delivery, surgery, sensing, and detoxification. *Sci. Robot.* **2** (2017).
- 2 Mallouk, T. E. & Sen, A. Powering Nanorobots. *Sci. Am.* **300**, 72-77 (2009).
- 3 Li, J., Rozen, I. & Wang, J. Rocket Science at the Nanoscale. *ACS Nano* **10**, 5619-5634, doi:10.1021/acsnano.6b02518 (2016).
- 4 Soler, L., Magdanz, V., Fomin, V. M., Sanchez, S. & Schmidt, O. G. Self-propelled micromotors for cleaning polluted water. *ACS Nano* **7**, 9611-9620 (2013).
- 5 Volpe, G. & Volpe, G. The topography of the environment alters the optimal search strategy for active particles. *Proceedings of the National Academy of Sciences* **114**, 11350-11355 (2017).
- 6 Sánchez, S., Soler, L. & Katuri, J. Chemically Powered Micro- and Nanomotors. *Angew. Chem. Int. Ed.* **54**, 1414-1444, doi:10.1002/anie.201406096 (2015).
- 7 Haeufle, D. F. B. *et al.* External control strategies for self-propelled particles: Optimizing navigational efficiency in the presence of limited resources. *Phys. Rev. E* **94**, 012617 (2016).
- 8 Yang, Y. & Bevan, M. A. Optimal Navigation of Self-Propelled Colloids. *ACS Nano* **12**, 10712-10724, doi:10.1021/acsnano.8b05371 (2018).
- 9 Haeufle, D. F. *et al.* External control strategies for self-propelled particles: Optimizing navigational efficiency in the presence of limited resources. *Phys. Rev. E* **94**, 012617 (2016).
- 10 Qian, B., Montiel, D., Bregulla, A., Cichos, F. & Yang, H. Harnessing thermal fluctuations for purposeful activities: the manipulation of single micro-swimmers by adaptive photon nudging. *Chem. Sci.* **4**, 1420-1429, doi:10.1039/C2SC21263C (2013).
- 11 Liebchen, B. & Löwen, H. Optimal Control Strategies for Active Particle Navigation. *arXiv preprint arXiv:1901.08382* (2019).
- 12 Silver, D. *et al.* Mastering the game of Go with deep neural networks and tree search. *Nature* **529**, 484 (2016).
- 13 Silver, D. *et al.* Mastering the game of go without human knowledge. *Nature* **550**, 354 (2017).
- 14 Levine, S., Finn, C., Darrell, T. & Abbeel, P. End-to-end training of deep visuomotor policies. *The Journal of Machine Learning Research* **17**, 1334-1373 (2016).
- 15 Lillicrap, T. P. *et al.* Continuous control with deep reinforcement learning. *arXiv preprint arXiv:1509.02971* (2015).
- 16 Popova, M., Isayev, O. & Tropsha, A. Deep reinforcement learning for de novo drug design. *Sci. Adv.* **4**, eaap7885 (2018).
- 17 Zhou, Z., Li, X. & Zare, R. N. Optimizing Chemical Reactions with Deep Reinforcement Learning. *ACS Central Science* **3**, 1337-1344, doi:10.1021/acscentsci.7b00492 (2017).
- 18 Komorowski, M., Celi, L. A., Badawi, O., Gordon, A. C. & Faisal, A. A. The Artificial Intelligence Clinician learns optimal treatment strategies for sepsis in intensive care. *Nat. Med.* **24**, 1716 (2018).
- 19 Verma, S., Novati, G. & Koumoutsakos, P. Efficient collective swimming by harnessing vortices through deep reinforcement learning. *Proceedings of the National Academy of Sciences* **115**, 5849-5854 (2018).
- 20 LeCun, Y., Bengio, Y. & Hinton, G. Deep learning. *Nature* **521**, 436, doi:10.1038/nature14539 (2015).
- 21 Sutton, R. S. & Barto, A. G. *Reinforcement learning: An introduction*. Vol. 1 (MIT press

- Cambridge, 1998).
- 22 Rumelhart, D. E., Hinton, G. E. & Williams, R. J. Learning representations by back-propagating errors. *Cognitive modeling* **5**, 1 (1988).
 - 23 Mnih, V. *et al.* Human-level control through deep reinforcement learning. *Nature* **518**, 529 (2015).
 - 24 Van Hasselt, H., Guez, A. & Silver, D. in *Thirtieth AAAI Conference on Artificial Intelligence*.
 - 25 Andrychowicz, M. *et al.* in *Adv. Neural Inf. Process. Syst.* 5048-5058.
 - 26 Krizhevsky, A., Sutskever, I. & Hinton, G. E. in *Adv. Neural Inf. Process. Syst.* 1097-1105.
 - 27 Puterman, M. L. *Markov Decision Processes: Discrete Stochastic Dynamic Programming*. (Wiley, 2014).
 - 28 Howse, J. R. *et al.* Self-motile colloidal particles: From directed propulsion to random walk. *Phys. Rev. Lett.* **99**, doi:ARTN 04810210.1103/PhysRevLett.99.048102 (2007).
 - 29 Maaten, L. v. d. & Hinton, G. Visualizing data using t-SNE. *Journal of machine learning research* **9**, 2579-2605 (2008).
 - 30 van Teeffelen, S. & Löwen, H. Dynamics of a Brownian circle swimmer. *Phys. Rev. E* **78**, 020101 (2008).
 - 31 Liu, Y., Yang, Y., Li, B. & Feng, X.-Q. Collective oscillation in dense suspension of self-propelled chiral rods. *Soft matter* (2019).
 - 32 Yang, Y. & Bevan, M. A. Interfacial colloidal rod dynamics: Coefficients, simulations, and analysis. *J. Chem. Phys.* **147**, 054902 (2017).
 - 33 Tang, X. *et al.* Optimal Feedback Controlled Assembly of Perfect Crystals. *ACS Nano* **10**, 6791-6798 (2016).
 - 34 Yang, Y. *Stochastic Modeling and Optimal Control for Colloidal Organization, Navigation, and Machines*, Johns Hopkins University, (2017).